Fault Feeder Identification in Non-effectively Grounded Distribution Network with Secondary Earth Fault

Shu Zhang, Tianlei Zang, Wenhai Zhang, and Xianyong Xiao

***Abstract*—Secondary earth faults occur frequently in power distribution networks under harsh weather conditions. Owing to its characteristics, a secondary earth fault is typically hidden within the transient of the first fault. Therefore, most researchers tend to focus on a feeder with single fault while disregarding secondary faults. This paper presents a fault feeder identification method that considers secondary earth faults in a non-effectively grounded distribution network. First, the wavelet singular entropy method is used to detect a secondary fault event. This method can identify the moment at which a secondary fault occurs. The zero-sequence current data can be categorized into two fault stages. The first and second fault stages correspond to the first and secondary faults, respectively. Subsequently, a similarity matrix containing the time-frequency transient information of the zero-sequence current at the two fault stages is defined to identify the fault feeders. Finally, to confirm the effectiveness and reliability of the proposed method, we conduct simulation experiments and an adaptability analysis based on an electromagnetic transient program.**

***Index Terms*—Secondary earth fault, non-effectively grounded distribution network, wavelet singular entropy, similarity matrix, zero-sequence current.**

I. Introduction

THE neutral point of the 6 kV to 66 kV power grid in China is generally either not grounded or grounded by arc-suppression coils. Therefore, the distribution network is also known to be non-effectively grounded [1]. The fault current is extremely low in magnitude because of isolated neutrality and can be further limited using arc-suppression coils if a single-phase-to-ground fault occurs in the resonant grounded network. In China, a non-effectively grounded distribution network is allowed to operate with a single-phase-to-ground fault for 1-2 hours to improve the reliability of the power supply [2]. However, during this period, the increase in the non-fault phase voltage threatens the system insulation and results in interphase short circuits, protection trips, and other issues. This can be prevented from worsening if the fault line is detected correctly. Therefore, the fault feeder from an array of feeders connected to the same bus must be quickly identified to reduce the time required to determine the fault location [3].

Many relevant studies regarding feeder fault identification have been conducted. State-of-the-art studies on this topic can be categorized into two groups [4]: fundamental frequency component based algorithms and transient signal based algorithms. Fundamental frequency component based algorithms may fail in resonant grounded distribution networks with an overcompensation state because the Petersen coil generates an inductive current that can compensate for the fault current. Hence, the steady-state characteristics of the zero-sequence current are similar between the fault feeder and healthy feeders [5]. However, the transient zero-sequence current of the fault line is several times larger than the steady-state zero-sequence current after the occurrence of a single-phase-to-ground fault, resulting in a significant amount of characteristic information of the specific fault [6]. For a more comprehensive understanding of this phenomenon, a range of transient signal based algorithms have been investigated extensively in recent years [7]. In general, the wavelet transform [8], S-transform [9], mathematical morphology [10], and Hilbert-Huang transform [11] are routinely used for extracting transient features of the zero-sequence current. In [12], the amplitude and polarity information of the transient zero-sequence current has been used to form the detection criteria. In [13], a comprehensive similarity coefficient has been used for the detection of fault lines. Recently, artificial-intelligence-based, fuzzy-inference-based, and optimization-based methods have provided effective protection against single-phase-to-ground faults [14], [15]. However, these protection methods only consider one of the feeders during a single-phase-to-ground fault [16].

Under the conditions of harsh weather or deteriorated insulation, secondary earth faults occur frequently [17], [18]. Reference [19] considers a number of blackout accidents that are known to cause secondary faults with different feeders in a distribution network with resonant earth fault in

Manuscript received: July 9, 2020; accepted: December 7, 2020. Date of CrossCheck: December 7, 2020. Date of online publication: February 17, 2021.

This work was supported in part by National Science Foundation of China (No. 51907097), National Key R&D Program of China (No. 2020YFF0305800), the Full-time Postdoc Research and Development Fund of Sichuan University in China (No. 2019SCU12003), and the Applied Basic Research of Sichuan Province (No. 2020YJ0012).

S. Zhang, T. Zang (corresponding author), W. Zhang, and X. Xiao are with the Department of Electrical Engineering, Sichuan University, Chengdu, China (e-mail: ZS20061621@163. com; zangtianlei@126. com; 649127529@qq. com; xiaoxianyong@163.com).

DOI: 10.35833/MPCE.2020.000466

Queensland, Australia. Moreover, similar failures with two single-phase-to-ground faults occurring at different feeders with the same phase have been reported in 10 kV and 6 kV distribution networks in China [20]. Consequently, the secondary fault can be defined as a new fault that occurs when the power system has not been adjusted to sufficiently healthy conditions after the first fault. Moreover, the two faults occur with a time difference because the faults do not occur simultaneously [21], [22]. Although a first failure does not necessarily result in a secondary failure, it will increase the elimination time of fault and continue to threaten the security of the system if the secondary failure cannot be identified. Moreover, the accuracy of the existing fault line selection devices in a non-effective grounded distribution network is not high, thereby increasing the risk of secondary failure. Therefore, it is important to identify secondary faults, particularly under harsh weather conditions. Most researchers in this field have focused on a feeder with single fault while disregarding secondary faults. In particular, for a non-effectively grounded distribution network, the fault current of the first fault is weak. Secondary faults may occur in either the same phase or a different phase between the two feeders. If the fault current of the secondary fault occurs in the same phase, it will be submerged in the first fault transient so that it is difficult to conduct subsequent identifications. Hence, the fault feeder identification method presented herein focuses only on secondary faults that occur in the same phase but with different feeders. Compared with the existing methods of fault feeder identification, the main contributions of this paper are as follows.

1) The proposed method focuses on secondary earth faults that occur in the same phase but with different feeders in a non-effectively grounded distribution network. Moreover, the features of the transient zero-sequence current of secondary earth faults are analyzed.

2) The peak of the wavelet singular entropy increment is defined as the criterion for identifying the fault time of a secondary earth fault. In addition, the fault process can be categorized into two stages. The first and second stages are for the first and secondary faults, respectively.

3) The similarity matrix contains separate time-frequency information of the fault for the two steps and must be defined to identify the fault feeders. The proposed method can reveal the development process of the fault and correctly identify the origin of the feeder with secondary earth fault.

4) The feeder identification method proposed herein is suitable not only for secondary earth faults, but also for a single-phase grounded fault, rendering it adaptable to different fault scenes.

The remainder of this paper is organized as follows. Section II provides an analysis of the features of the transient zero-sequence current of secondary earth faults. In Section III, the scheme and algorithm of fault feeder identification are presented. The method is tested via simulation, and the associated assessments under different fault conditions are introduced in Section IV. Finally, a brief conclusion is presented in Section V.

II. Features of Transient Zero-sequence Current of Secondary Earth Faults

When a single-phase-to-ground fault F_1 occurs in feeder k of the resonant grounded network, the transient grounding current i_d, as shown in Fig. 1, is constituted by a transient capacitive current i_C and transient inductive current i_L, as shown in (1) [2].

$$i_d = i_C + i_L = (I_{Cm} - I_{Lm})\cos(\omega t + \varphi) + I_{Lm}\cos\varphi \mathrm{e}^{-\frac{t}{\tau_L}} + I_{Cm}\left(\frac{\omega_f}{\omega}\sin\varphi\sin(\omega t) - \cos\varphi\cos(\omega_f t)\right)\mathrm{e}^{-\frac{t}{\tau_C}} \quad (1)$$

where I_{Cm} and I_{Lm} are the magnitudes of the capacitive and inductive currents, respectively; ω is the power angular frequency; φ is the initial phase angle of the phase voltage at the fault time; ω_f is the angular frequency of the free oscillation component; and τ_C and τ_L are the time constants of the capacitance and inductance loops, respectively. In (1), the first part is the steady-state component of the transient grounding current, which is the difference between the steady-state capacitive current and steady-state inductive current. The second and third parts are the transient components of the transient grounding current, which is the sum of the transient free oscillation component of the capacitor current and the transient direct current component of the inductive current. As the two transient currents may be superimposed on each other, the amplitude of i_d is substantially increased.

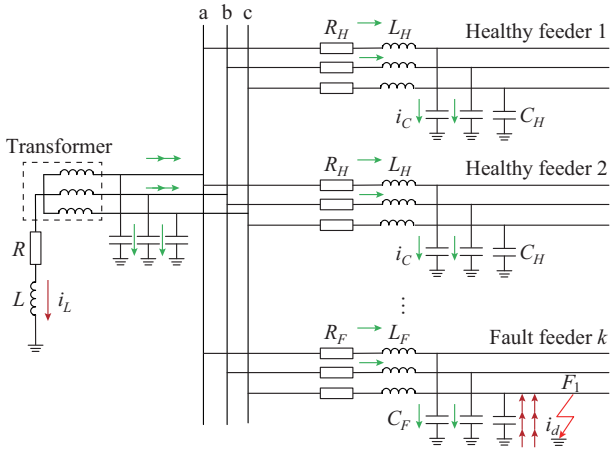

Fig. 1. Current distribution of single-phase grounded fault in resonant grounded distribution network.

In Fig. 1, R and L are the resistance and inductance of arc-suppression coil, respectively; R_H, L_H, and C_H are the resistance, inductance, and capacitance of healthy feeders, respectively; and R_F, L_F, and C_F are the resistance, inductance, and capacitance of the fault feeder, respectively.

When the secondary earth fault F_2 occurs in feeder 1, based on the fault conditions shown in Fig. 1, the zero-sequence network with secondary faults is shown in Fig. 2. In Fig. 2, U_{f10} and U_{f20} are the zero-sequence sources of F_1 and F_2, respectively; R_{f1} and R_{f2} are the fault resistances of the first and secondary faults, respectively; and I_{01}, I_{02}, …, I_{0k} are the zero-sequence currents of feeders 1, 2, …, k, respectively. The equivalent circuit of a zero-sequence network after

the occurrence of secondary earth fault F_2 is shown in Fig. 3, where the impedance of the healthy feeders Z_H and the impedance of the arc-suppression coil Z_L are significantly greater than those of the fault feeders. Hence, Z_H and Z_L can be disregarded in the approximate calculation.

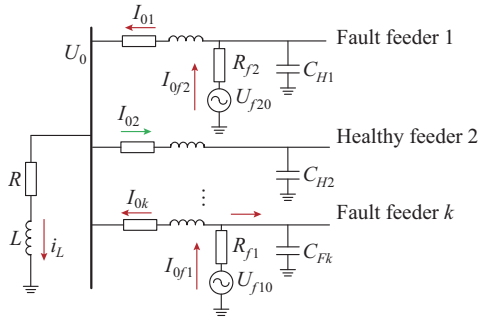

Fig. 2. Simplified diagram of zero-sequence network for single-phase-to-ground fault with secondary faults.

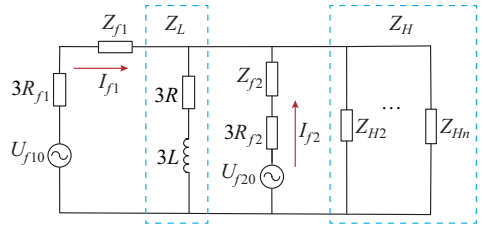

Fig. 3. Equivalent circuit of zero-sequence network.

Therefore, the zero-sequence current after the secondary earth fault F_2 can be expressed as:

$$I_f = \frac{U_{f10}}{Z_H//(Z_{f2}+3R_{f2})//Z_L+Z_{f1}+3R_{f1}} - \frac{U_{f20}}{Z_H//(Z_{f1}+3R_{f1})//Z_L+Z_{f2}+3R_{f2}} \approx \frac{U_{f10}-U_{f20}}{3R_{f1}+Z_{f1}+Z_{f2}+3R_{f2}} \tag{2}$$

where I_f is the zero-sequence current; and Z_{f1} and Z_{f2} are the line impedances of feeders with the first and secondary faults, respectively.

In (2), U_{f10} is similar to U_{f20} because the secondary earth faults occur in the same phase but from different feeders. The zero-sequence current I_f is extremely small. Therefore, it is difficult to detect the feeder with secondary fault. The waveforms of the zero-sequence current with secondary faults in a resonant grounded network with four feeders are presented in Fig. 4.

In Fig. 4, the first single-phase-to-ground fault occurs in feeder 1 at 0.215 s, and the secondary fault on the same phase occurs in feeder 2 at 0.225 s. As shown in Fig. 4, the transients of the first fault are significant, and the current phases of the healthy feeders (feeders 2, 3, and 4) at the first fault time are almost identical, with only variations in the amplitude. However, the transient of the secondary fault is extremely weak and almost hidden within the fault current. As the secondary fault occurs in feeder 2, the zero-sequence current of feeder 2 is presented separately in Fig. 4. The transient of the secondary fault is superimposed on the capacitive current. An abrupt change in the zero-sequence current occurs during the secondary fault. Since the original capacitive current is small, the zero-sequence current after the secondary fault is similar to the steady current after the first fault. Therefore, the transients of the feeders with secondary faults are disregarded, resulting in the misidentification of fault feeders.

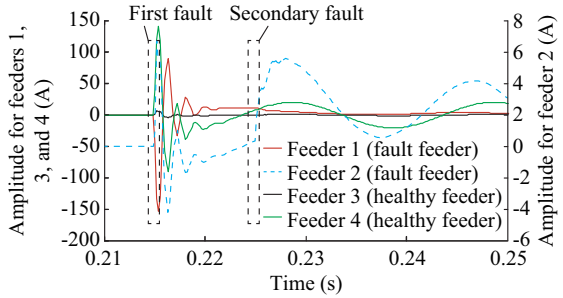

Fig. 4. Waveforms of zero-sequence current with secondary faults.

Although it is difficult to detect the amplitude of the transient zero-sequence current of the secondary fault, the two fault transient components are in the fault current. A new source is added to the first state, resulting in more complex modes of the transient signal, as shown in (2). Therefore, the complexity of the fault network increases after the occurrence of a secondary fault.

III. Scheme and Algorithm of Fault Feeder Identification

A. Detection of Secondary Fault on the Same Phase

Based on the analysis of secondary faults, an indicator is necessitated to quantify the complexity of the zero-sequence current for detecting secondary faults. In this paper, the wavelet singular entropy (WSE) is used to assess the complexity of the transient signal in different fault states. The analyzed zero-sequence current $I_0[n]$ is expressed as a time sequence containing N samples. Next, a wavelet decomposition matrix $\boldsymbol{D}$ with $m \times n$ orders can be obtained via a wavelet transform. Based on the singular value decomposition theory for signals, the calculated diagonal elements $\lambda_i (i = 1, 2, \ldots, l)$ are singular values $\boldsymbol{D}_{m\times n}$. Therefore, WSE can be expressed as [23]:

$$WSE = \sum_{i=1}^{l} \Delta p_i \tag{3}$$

where Δp_i is the incremental WSE of the i^{th} non-zero singular value. The singular value decomposition of the wavelet transform result is equivalent to mapping the correlated wavelet space to a linearly independent feature space. Combining the redundant information, the WSE indicates the distribution uncertainty of the energy in the signal time-frequency space. The more modes in which the energy congregates, the greater the WSE is. Therefore, the WSE of a zero-sequence current can be used as an index to measure the signal complexity and uncertainty. As the occurrence of secondary fault is continuous, the WSE sequence W_E is defined as:

$$W_E = \{WSE(1), WSE(2), \ldots, WSE(g), \ldots, WSE(G)\} \quad G = N/q \tag{4}$$

where $WSE(g)$ is the WSE of the g^{th} data window; q is the length of the data window for calculating the WSE, and is selected as 8; and G is the number of data windows. In this paper, when a secondary fault occurs in the distribution network, two fault transients are contained in the fault current with different fault times. Theoretically, the value of WSE decreases because of the first fault transient attenuation, and then increases as the secondary fault occurs. The WSEs of zero-sequence currents for the four feeders, as mentioned above, are shown in Fig. 5.

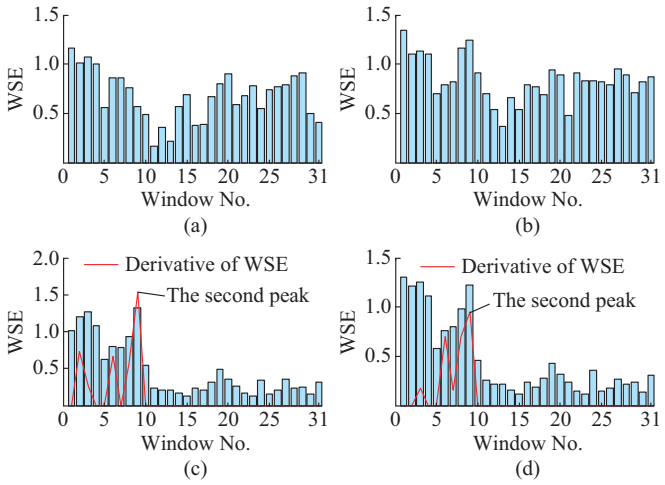

Fig. 5. WSE of zero-sequence currents. (a) Feeder 1. (b) Feeder 2. (c) Feeder 3. (d) Feeder 4.

The value of the entropy varies with the sliding window, where the two feeders with the closest WSE are selected as the basis for detecting secondary faults. Equation (5) is used to compare the entropy curves of every feeder.

$$Q_{ij} = \sqrt{\frac{1}{G}\sum_{g=1}^{G}(WSE_i(g) - WSE_j(g))^2} \tag{5}$$

where Q_{ij} is the similarity of WSE between feeder i and feeder j; and WSE_i and WSE_j are the WSE of feeder i and feeder j, respectively. Feeder i and feeder j are any two feeders from the bus. As shown in Fig. 5, feeders 3 and 4 exhibit similar entropy curves. Notably, the entropy value is extremely small after the 10^{th} sliding window. To avoid false judgments caused by invalid entropy changes, a threshold σ is set to filter the smaller values of the WSE, i.e., $\sigma = 0.5$. As mentioned in the previous analysis, the occurrence of secondary faults increases the complexity of fault signals. This implies that a positive mutation is reflected in the entropy curve, as shown by the red line in Fig. 5. The largest mutation point of the entropy curve is defined as the second peak of the WSE because the first peak is at the first fault time.

$$WSE_{peak} = \max\left((WSE(g) - WSE(g-1))/\Delta t\right) \tag{6}$$

where Δt is the time of the data window; $WSE_{peak} > 0$; and $WSE(g) > \sigma$. As shown in Fig. 5, the 9^{th} data window is the second peak value of the singular entropy of feeders 3 and 4. Based on the sample frequency, the time of the secondary fault is 0.22512 s.

B. Proposed Fault Feeder Identification Method Involving Secondary Fault

Based on the detection result of the secondary fault, the fault-time interval can be categorized into two stages. The first stage $[t_{start}, t_{second}]$ is for the first single-phase-to-ground fault, whereas the second stage $[t_{second}, t_{end}]$ is for the second single-phase-to-ground fault, where t_{start} is the first fault occurrence time, which typically depends on the zero-sequence voltage exceeding the threshold value [24]; t_{second} is the secondary fault occurrence time; and t_{end} is the end time of fault detection. Depending on the approach used to analyze the fault circuit, the zero-sequence current of the healthy feeder is primarily composed of its own zero-sequence capacitance. Therefore, the current waveforms among healthy feeders are highly similar, and the similarity is closely associated with the length and type of feeders [25]. A similarity index of time-frequency matrices [26] using a wavelet transform can be used to identify the fault feeders. The time-frequency matrix $\boldsymbol{E}$ is calculated using the integral of the wavelet coefficients in its high-frequency details, as expressed as:

$$\boldsymbol{E} = \begin{bmatrix} D(1,1)\Delta t & D(1,2)\Delta t & \cdots & D(1,n)\Delta t \\ D(2,1)\Delta t & D(2,2)\Delta t & \cdots & D(2,n)\Delta t \\ \vdots & \vdots & & \vdots \\ D(m,1)\Delta t & D(m,2)\Delta t & \cdots & D(m,n)\Delta t \end{bmatrix} \tag{7}$$

Therefore, based on (7), the time-frequency matrix $\boldsymbol{EE}$ at the two stages of each feeder can be obtained as:

$$\boldsymbol{EE} = \begin{bmatrix} \boldsymbol{E}_1^1 & \boldsymbol{E}_2^1 & \cdots & \boldsymbol{E}_k^1 \\ \boldsymbol{E}_1^2 & \boldsymbol{E}_2^2 & \cdots & \boldsymbol{E}_k^2 \end{bmatrix} \tag{8}$$

where $\boldsymbol{E}_k^1$ and $\boldsymbol{E}_k^2$ are the time-frequency matrices at the first and second stages of the feeder k, respectively. The similarity matrix $\boldsymbol{PP}$ can be defined as:

$$\boldsymbol{PP} = \begin{bmatrix} \frac{1}{K-1}\left(\sum_{j=1}^{K} S_{1j}^1 - S_{1,\max}^1\right) & \frac{1}{K-1}\left(\sum_{j=1}^{K} S_{2j}^1 - S_{2,\max}^1\right) & \cdots & \frac{1}{K-1}\left(\sum_{j=1}^{K} S_{kj}^1 - S_{k,\max}^1\right) \\ \frac{1}{K-1}\left(\sum_{j=1}^{K} S_{1j}^2 - S_{1,\max}^2\right) & \frac{1}{K-1}\left(\sum_{j=1}^{K} S_{2j}^2 - S_{2,\max}^2\right) & \cdots & \frac{1}{K-1}\left(\sum_{j=1}^{K} S_{kj}^2 - S_{k,\max}^2\right) \end{bmatrix} \tag{9}$$

where S_{kj}^1 and S_{kj}^2 are the similarities of feeder k and arbitrary feeder j at the first and second stages, respectively; $S_{k,\max}^1$ and $S_{k,\max}^2$ are the maximum values of the similarity between feeder k and the other feeder at the first and second stages, respectively; and K is the total number of feeders. The formula used for this calculation is presented in (10).

$$S_{ij} = \frac{\sum_{m=1}^{M}\sum_{n=1}^{N} E_i(m,n)E_j(m,n)}{\sqrt{\sum_{m=1}^{M}\sum_{n=1}^{N} E_i^2(m,n)E_j^2(m,n)}} \tag{10}$$

where S_{ij} is the similarity of time-frequency matrices be-

tween feeder i and feeder j; $E_i(m,n)$ and $E_j(m,n)$ are the elements of time-frequency matrices of feeder i and feeder j, respectively; and M and N are the rows and columns of the time-frequency matrices, respectively. The similarity matrix ***PP*** defined in (9) can be used to identify fault feeders. $PP(,i)$ refers to the value of column i of any row in the matrix ***PP***. If $PP(,i)$ is closer to 1, the feeder is more likely to be a healthy feeder. Otherwise, if the value of $PP(,i)$ is smaller, the feeder is more likely to be a fault feeder. To identify the fault feeder, $PP(,i)$ is compared with a threshold k_{set}, which is equal to zero in this paper.

The flow chart of the proposed fault line identification process in the distribution network considering secondary faults is shown in Fig. 6.

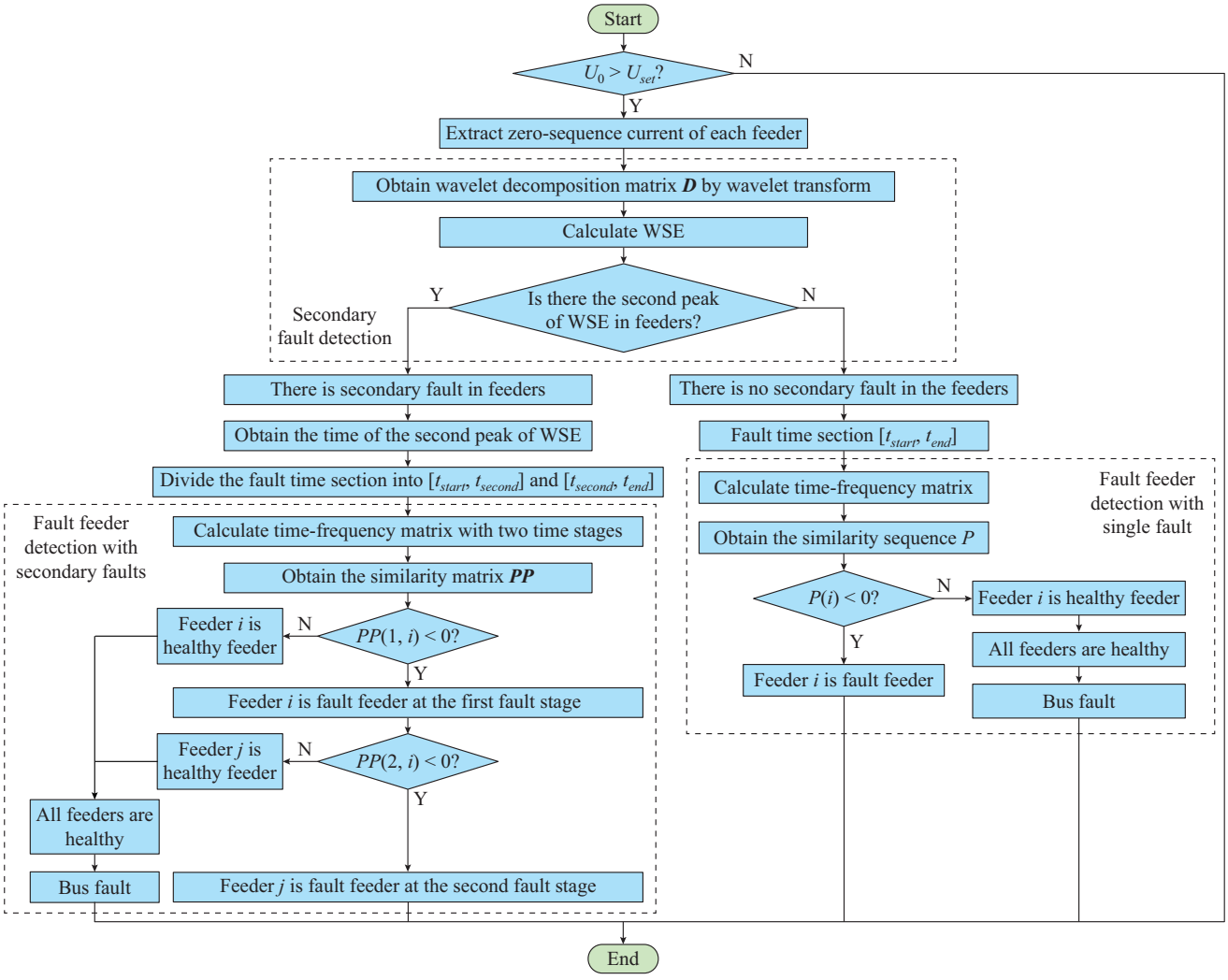

Fig. 6. Flow chart of proposed fault feeder identification process.

The detailed procedures for this process are as follows.

Step 1: when the zero-sequence voltage U_0 exceeds the threshold U_{set}, the fault feeder identification program is initiated. Typically, the fault threshold is set to be 15% of the phase voltage.

Step 2: the process moves into the secondary fault detection stage. The zero-sequence current of each feeder is extracted in two cycles. The wavelet decomposition matrix ***D*** is obtained using a wavelet transform.

Step 3: the WSE is calculated using a sliding data window, and the sequence W_E of each feeder is obtained. Subsequently, the root-mean-square (RMS) error of W_E for any two feeders is calculated, and two feeders with the minimum RMS error are selected. The time of the secondary fault at which the value of the entropy increases the most is extracted, and this time is labelled as the second peak of the WSE. If a secondary fault cannot be detected, jump to *Step 6*.

Step 4: the time section is categorized into two steps, $[t_{start}, t_{second}]$ and $[t_{second}, t_{end}]$, and the similarity matrix ***PP*** is calculated. If $PP(1,i)<0$, feeder i is the fault feeder at the first fault stage. Otherwise, feeder i is a healthy feeder. If all $PP(1,i)>0$, then the first fault occurs on the bus.

Step 5: continue to assess $PP(2,i)$. If $PP(2,j)<0, j\neq i$, feeder j is the fault feeder at the secondary fault stage. Otherwise, feeder j is a healthy feeder. If all $PP(2,i)>0$, it implies that a secondary fault occurs on the bus.

Step 6: in the time section $[t_{start}, t_{end}]$, the similarity matrix ***PP*** is calculated, where ***PP*** is a one-dimensional sequence. ***P*** is defined as the similarity sequence in the condition without secondary fault. If $P(i)<0$, feeder i is the fault feeder. Otherwise, feeder i is a healthy feeder. If all $P(i)>0$, it im-

plies that a fault occurs on the bus.

IV. Simulation Tests and Analysis

A. Simulation Models

The PSCAD/EMTDC simulation model used for a typical 35 kV distribution network with a resonant grounded network is shown in Fig. 7, where CT and PT are the current transformer and voltage transformer, respectively.

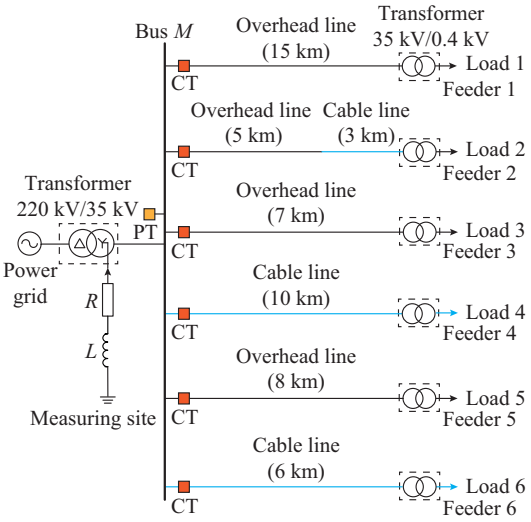

Fig. 7. 35 kV distribution network with resonant grounded system.

Six feeders are used in the system, in addition to three overhead lines of 15, 7, and 8 km, and two cable lines of 10 and 6 km. One line includes an overhead line of 5 km and a cable line of 5 km. The zero-sequence parameters of the overhead line are $Z_0=(0.517+\mathrm{j}1.485)\Omega/\mathrm{km}$ and $Y_0=\mathrm{j}1.476$ μs/km. The zero-sequence parameters of the cable line are $Z_0=(0.562+\mathrm{j}0.277)\Omega/\mathrm{km}$ and $Y_0=\mathrm{j}132$ μs/km. For Petersen coil grounding methods, the system is set to overcompensate with an overcompensation degree of 108%. Based on the distribution capacitance of the system to the ground, the Petersen coil inductance L can be calculated using (11), where C_{all} is the equivalent capacitance of total transmission lines. The active power loss of the Petersen coil is 3% of the inductance power loss. Hence, the series resistance can be calculated as:

$$L=\frac{1}{1.08\times(3\omega^2C_{all})}=0.5223\,\mathrm{H} \tag{11}$$

$$R=0.03\omega L=4.9226\,\Omega \tag{12}$$

B. Simulation Results

1) Secondary Faults

To verify the effectiveness of the fault feeder identification method that considers secondary faults, a phase-grounded fault is generated in feeder 1 at 0.215 s, and a secondary fault is generated in feeder 3 at 0.225 s with the same phase. The resistance of each fault is 50 Ω. If the fault feeder identification is performed without the detection of a secondary fault, the similarity index of the time-frequency matrices is used to detect the first fault feeder. The time-frequency matrices of every feeder in one cycle can be calculated as shown in Fig. 8, in which the similarity sequence is:

$$\boldsymbol{P}=[-0.7719\quad 0.4458\quad 0.1341\quad 0.4603\quad 0.4607\quad 0.4603] \tag{13}$$

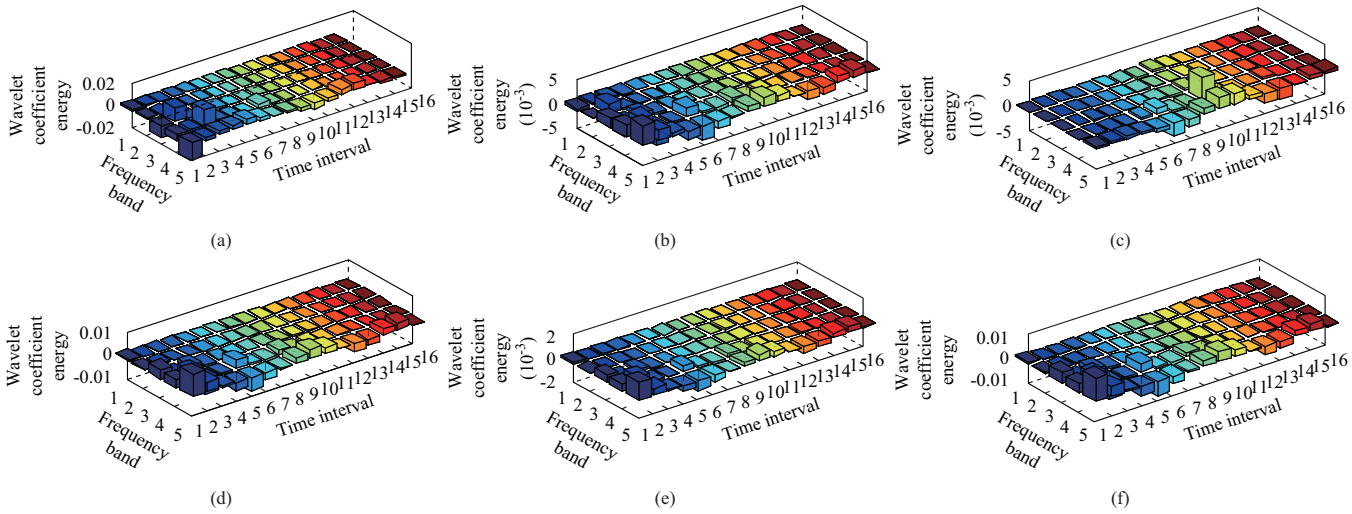

Fig. 8. Time-frequency matrices of every feeder in one cycle. (a) Feeder 1. (b) Feeder 2. (c) Feeder 3. (d) Feeder 4. (e) Feeder 5. (f) Feeder 6.

In this case, only feeder 1 is identified as the fault feeder. Based on the proposed process of fault feeder identification in which the secondary faults are considered, the WSE of every feeder is shown in Fig. 9. Feeders 4 and 6 indicate the smallest RMS errors in W_E. Simultaneously, the 8th window is detected as the second peak of the WSE. Therefore, 0.2238 s is considered to be the time at which a secondary fault occurs. The time-frequency matrices of the first and second stages are shown in Fig. 10(a) and 10(b), respectively. The similarity matrix ***PP*** is determined as follows. When $PP(1,1)<0$, feeder 1 is regarded as the fault feeder at the first fault stage. Similarly, since $PP(2,1)<0$ and $PP(2,3)<0$ at the second fault stage, feeder 3 is regarded as the secondary fault feeder. Simultaneously, the development process of

the secondary faults can be obtained using the similarity matrix ***PP***. Accordingly, the single-phase-to-ground fault occurs in feeder 1 first, and then a secondary fault with the same phase occurs in feeder 3 after half of the cycle.

$$\boldsymbol{PP}=\begin{bmatrix}-0.7651 & 0.4276 & 0.1104 & 0.4431 & 0.4432 & 0.4431\\ -0.2066 & 0.3916 & -0.2219 & 0.3984 & 0.4014 & 0.3984\end{bmatrix} \quad (14)$$

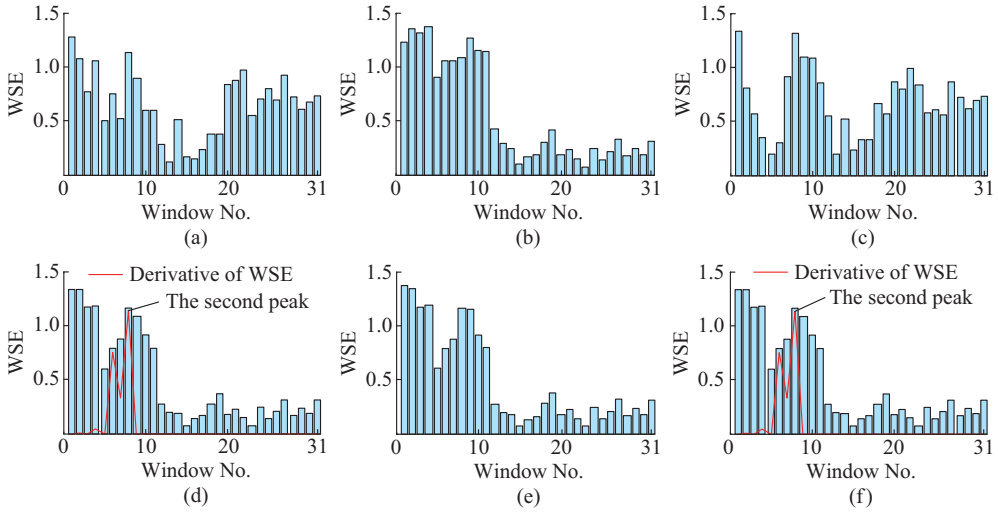

Fig. 9. WSE of zero-sequence currents considering secondary fault. (a) Feeder 1. (b) Feeder 2. (c) Feeder 3. (d) Feeder 4. (e) Feeder 5. (f) Feeder 6.

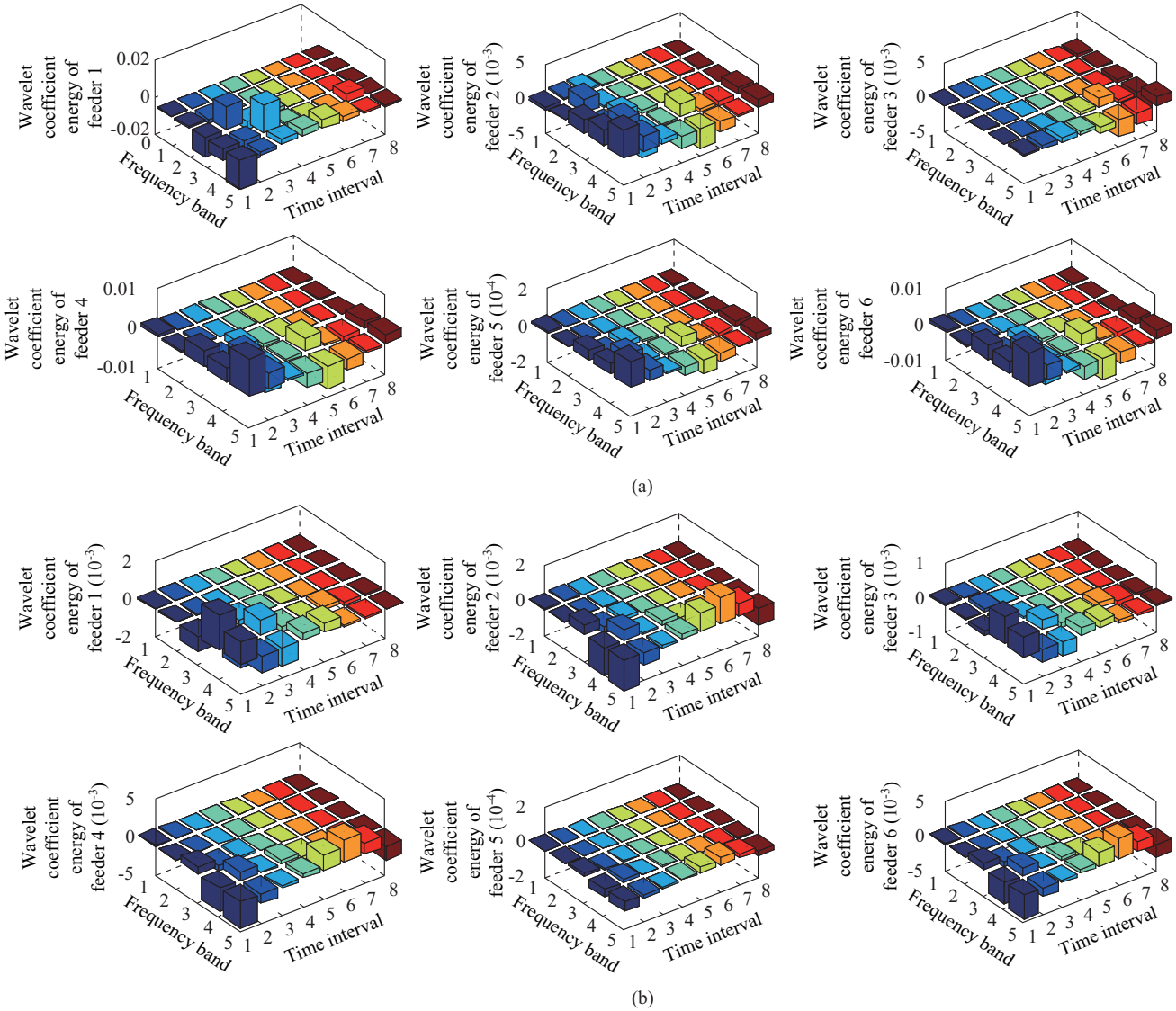

Fig. 10. Time-frequency matrices of every feeder at both fault stages. (a) First fault stage. (b) Second fault stage.

2) Single-phase-to-ground Fault

The proposed method focuses on secondary faults, which often occur under harsh weather conditions. However, single-phase-to-ground fault occurs frequently in a distribution network. To verify the effectiveness of the fault feeder identification method, a single-phase-to-ground fault is generated in feeder 1 at 0.215 s, and the fault resistance is 100 Ω. The WSE is shown in Fig. 11. The second peak could not be detected by the WSE of the zero-sequence current. Therefore, only a single fault occurs in the feeders, and the time section must not be divided. Based on (9), the similarity sequence can be calculated as:

$$\boldsymbol{P}=[\,-0.9667\;\;0.5909\;\;0.6017\;\;0.6012\;\;0.6021\;\;0.6012\,] \tag{15}$$

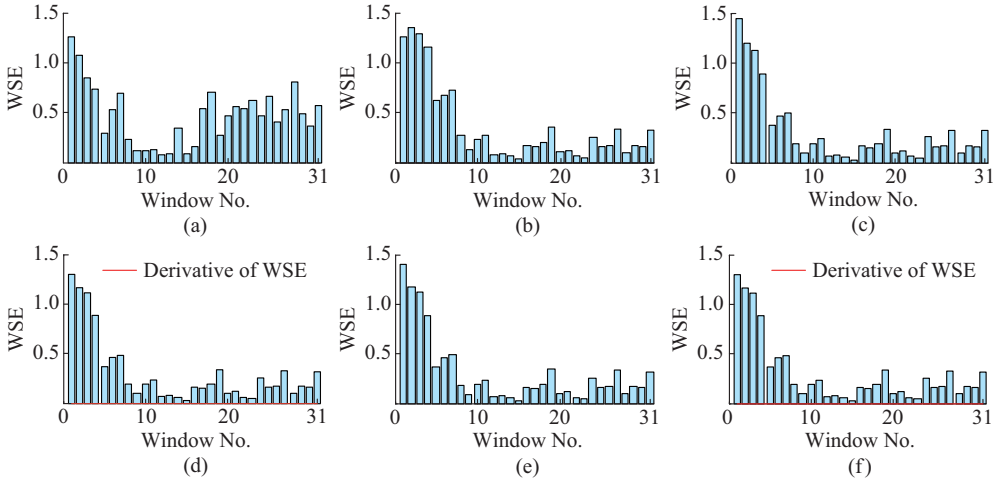

Fig. 11. WSE of zero-sequence with single fault. (a) Feeder 1. (b) Feeder 2. (c) Feeder 3. (d) Feeder 4. (e) Feeder 5. (f) Feeder 6.

Since $P(1)<0$, feeder 1 can be regarded as the fault feeder. Based on the simulation analysis above, the feeder identification method is not only suitable for secondary earth faults, but also for a single-phase-to-ground fault, rendering it adaptable to different fault scenes.

C. Sensitivity Assessment

1) Different Initial Angles and Fault Feeders

The detection results of the secondary faults with different initial fault angles of the fault feeders are shown in Table I, where the columns of F_1 and F_2 in Table I refer to the feeders of the first fault and the secondary fault, respectively; T_1 and T_2 are the actual fault time of the first fault and the secondary fault, respectively; and T is the detected fault time of the secondary fault. The faults occur in feeders 1-6. The secondary faults occur at 0.223, 0.225, 0.240, and 0.245 s. Table I shows that the time at which the secondary fault is detected has a slight error compared with the actual fault time. Because of the sliding data window of the WSE, the secondary fault feeder can be detected correctly. Using the secondary faults that occur in feeders 4 and 5 as examples, the first fault occurs at 0.215 s with a fault resistance of 400 Ω. The second single-phase-to-ground fault occurs at 0.245 s, with a fault resistance of 500 Ω. The secondary fault time is determined to be 0.2456 s using the WSE method. The similarity matrix is calculated as:

$$\boldsymbol{PP}=\begin{bmatrix}0.5970 & 0.5942 & 0.6082 & -0.6210 & 0.3662 & 0.6010\\ 0.6316 & 0.6323 & 0.6331 & 0.6437 & -0.8110 & 0.6326\end{bmatrix} \tag{16}$$

Hence, feeders 4 and 5 are detected as the fault feeders at the first and second fault stages, respectively.

Additionally, the proposed method is suitable for bus faults and high-impedance faults (HIFs), as detailed in Table I. Using bus M as an example, a single-phase-to-ground fault occurs in feeder 1 at a distance of 0.215 s (0.5 km) from bus M, which is at the head of the feeder, and a secondary fault occurs at bus M at 0.225 s. The WSE is shown in Fig. 12.

As the WSEs of feeders 5 and 6 are the most similar, the 8th data window is the maximum point of the wavelet entropy increment of feeders 5 and 6. Therefore, the 8th window after the first fault with 64 samples is considered to be the time at which a secondary fault occurs. The time-frequency matrices $\boldsymbol{PP}$ of the first and second stages are shown as:

$$\boldsymbol{PP}=\begin{bmatrix}-0.9970 & 0.5917 & 0.5976 & 0.5979 & 0.5978 & 0.5979\\ 0.4225 & 0.8760 & 0.8681 & 0.8808 & 0.8745 & 0.8854\end{bmatrix} \tag{17}$$

Based on the criterion $PP(1,1)<0$, feeder 1 is regarded as the fault feeder at the first fault stage. At the second fault stage, none of the feeders exhibit a value less than 0 in the time-frequency matrices $\boldsymbol{PP}$. Thus, we can conclude that a secondary fault occurs at bus M.

Notably, two parameters exhibit values less than 0 in some cases, whereas only one parameter exhibits a value less than 0 in some cases at the second fault stage. This is because two fault feeders are used at the second fault stage, one for the first fault stage and the other for the second fault stage. If the fault transient produced from the first fault stage continues to the second fault stage, the values of the two parameters will be less than 0 in $PP(2,i)$. Otherwise, if the fault transient produced from the first fault has been attenuated to a certain extent, only one secondary fault feeder will be detected at the second fault stage. In fact, the transient duration and magnitude are affected by the fault resistance, fault time, and transmission lines. Therefore, the number of parameters less than 0 in $PP(2,i)$ depends on the transient component at the first fault stage.

TABLE I
DETECTION RESULTS OF SECONDARY FAULTS WITH DIFFERENT FAULT INITIAL ANGLES AND FAULT FEEDERS

First fault stage			Second fault stage			Detection result of secondary faults	
F_1	R_1 (Ω)	T_1 (s)	F_2	R_2 (Ω)	T_2 (s)	T (s)	***PP***
1	50	0.215	2	0	0.223	0.2238	$\begin{bmatrix}-0.8498 & 0.1938 & 0.4967 & 0.4992 & 0.4991 & 0.4992\\ -0.3275 & -0.0766 & 0.5413 & 0.5418 & 0.5421 & 0.5418\end{bmatrix}$
1	5	0.215	3	200	0.223	0.2238	$\begin{bmatrix}-0.7820 & 0.4712 & 0.2808 & 0.4848 & 0.4850 & 0.4848\\ -0.3460 & 0.3537 & -0.2471 & 0.3530 & 0.3536 & 0.3530\end{bmatrix}$
1	200	0.215	5	200	0.223	0.2238	$\begin{bmatrix}-0.9011 & 0.4902 & 0.4927 & 0.4941 & 0.2680 & 0.4937\\ -0.5264 & 0.2350 & 0.2319 & 0.2344 & -0.5362 & 0.2345\end{bmatrix}$
4	50	0.215	1	50	0.223	0.2238	$\begin{bmatrix}0.5195 & 0.4239 & 0.5080 & -0.6930 & 0.4997 & 0.5500\\ -0.2065 & 0.7450 & 0.7534 & 0.6187 & 0.7532 & 0.7525\end{bmatrix}$
1	100	0.215	6	0	0.225	0.2251	$\begin{bmatrix}-0.8941 & 0.5519 & 0.5535 & 0.5588 & 0.5370 & 0.4091\\ -0.3769 & 0.2838 & 0.2969 & 0.2974 & 0.2896 & -0.4676\end{bmatrix}$
2	100	0.215	3	100	0.225	0.2251	$\begin{bmatrix}0.6103 & -0.9488 & 0.6105 & 0.6100 & 0.6101 & 0.6100\\ 0.5911 & 0.3552 & -0.6893 & 0.5919 & 0.5920 & 0.5919\end{bmatrix}$
2	0	0.215	5	100	0.225	0.2251	$\begin{bmatrix}0.5970 & -0.9869 & 0.5968 & 0.5970 & 0.5899 & 0.5970\\ 0.5482 & 0.3062 & 0.5468 & 0.5481 & -0.5865 & 0.5481\end{bmatrix}$
4	200	0.215	6	50	0.225	0.2251	$\begin{bmatrix}0.5813 & 0.5527 & 0.5884 & -0.9433 & 0.5871 & 0.5869\\ 0.7240 & 0.7232 & 0.7314 & 0.5435 & 0.7311 & -0.2752\end{bmatrix}$
3	400	0.215	5	200	0.240	0.2392	$\begin{bmatrix}0.5986 & 0.5889 & -0.9862 & 0.5983 & 0.5968 & 0.5983\\ 0.4479 & 0.4548 & 0.0108 & 0.4509 & -0.2454 & 0.4509\end{bmatrix}$
4	0	0.215	2	0	0.240	0.2418	$\begin{bmatrix}0.5614 & 0.5608 & 0.5816 & -0.9583 & 0.5813 & 0.5812\\ 0.6971 & -0.5107 & 0.6962 & 0.6051 & 0.6971 & 0.6966\end{bmatrix}$
4	400	0.215	3	200	0.240	0.2392	$\begin{bmatrix}0.5178 & 0.5141 & 0.2205 & -0.5093 & 0.5304 & 0.5207\\ 0.6745 & 0.6760 & -0.6135 & 0.6818 & 0.6766 & 0.6758\end{bmatrix}$
4	400	0.215	5	500	0.245	0.2456	$\begin{bmatrix}0.5970 & 0.5942 & 0.6082 & -0.6210 & 0.3662 & 0.6010\\ 0.6316 & 0.6323 & 0.6331 & 0.6437 & -0.8110 & 0.6326\end{bmatrix}$
5	600	0.215	6	0	0.245	0.2456	$\begin{bmatrix}0.6052 & 0.5985 & 0.6027 & 0.6054 & -0.9373 & 0.5816\\ 0.5992 & 0.5074 & 0.6493 & 0.6526 & 0.6059 & -0.4370\end{bmatrix}$
6	0	0.215	2	0	0.225	0.2264	$\begin{bmatrix}0.5150 & 0.5422 & 0.5603 & 0.5547 & 0.5591 & -0.9489\\ 0.6834 & -0.0759 & 0.6832 & 0.6833 & 0.6834 & 0.0447\end{bmatrix}$
6	0	0.215	3	0	0.245	0.2456	$\begin{bmatrix}0.5591 & 0.5586 & 0.5744 & 0.5787 & 0.5787 & -0.9548\\ 0.7272 & 0.7270 & -0.0509 & 0.7270 & 0.7272 & 0.2448\end{bmatrix}$
1	50	0.215	Bus	50	0.225	0.2251	$\begin{bmatrix}-0.9970 & 0.5917 & 0.5976 & 0.5979 & 0.5978 & 0.5979\\ 0.4225 & 0.8760 & 0.8681 & 0.8808 & 0.8745 & 0.8854\end{bmatrix}$
1	HIF	0.215	3	HIF	0.245	0.2444	$\begin{bmatrix}-0.9715 & 0.5855 & 0.5978 & 0.5947 & 0.5977 & 0.5913\\ -0.5866 & 0.2256 & -0.5590 & 0.2257 & 0.2261 & 0.2262\end{bmatrix}$

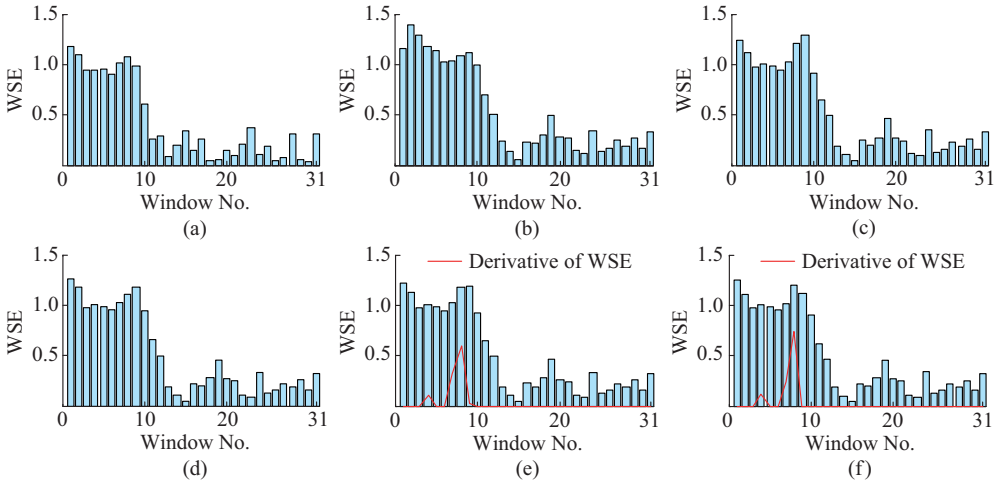

Fig. 12. WSE of zero-sequence currents with bus faults. (a) Feeder 1. (b) Feeder 2. (c) Feeder 3. (d) Feeder 4. (e) Feeder 5. (f) Feeder 6.

However, regardless of whether $PP(2,i)$ contains the fault feeder at the first fault stage, it will have one element whose value is less than 0, which thereby corresponds to the fault feeder of the secondary fault. Combined with $PP(1,i)$, we can obtain the development process of the secondary fault.

2) Different Grounding Resistance Values

This section presents the detection of secondary faults with different grounding resistance values. As shown in Table II, faults occur in feeders 3 and 5. The fault resistance is between 0 and 200 Ω. The simulation results in Table II show that the first and secondary faults can be correctly identified.

TABLE II
DETECTION RESULTS OF SECONDARY FAULTS WITH DIFFERENT GROUNDING RESISTANCES

First fault stage			Second fault stage			Detection result of secondary faults	
F_1	R_1 (Ω)	T_1 (s)	F_2	R_2 (Ω)	T_2 (s)	T (s)	***PP***
3	0	0.215	5	0	0.225	0.2251	$\begin{bmatrix}0.5808 & 0.5762 & -0.9720 & 0.5809 & 0.5466 & 0.5809\\ 0.5507 & 0.5391 & -0.0216 & 0.5498 & -0.0298 & 0.5498\end{bmatrix}$
				50		0.2251	$\begin{bmatrix}0.5906 & 0.5859 & -0.9824 & 0.5907 & 0.5752 & 0.5907\\ 0.5443 & 0.5423 & -0.1980 & 0.5439 & -0.2888 & 0.5439\end{bmatrix}$
				100		0.2251	$\begin{bmatrix}0.5947 & 0.5900 & -0.9870 & 0.5948 & 0.5871 & 0.5948\\ 0.5680 & 0.5659 & -0.2866 & 0.5677 & -0.1313 & 0.5677\end{bmatrix}$
				200		0.2251	$\begin{bmatrix}0.5977 & 0.5929 & -0.9904 & 0.5978 & 0.5953 & 0.5978\\ 0.5732 & 0.5710 & -0.3102 & 0.5730 & -0.0887 & 0.5730\end{bmatrix}$
3	50	0.215	5	0	0.225	0.2251	$\begin{bmatrix}0.4472 & 0.4471 & -0.7394 & 0.4483 & 0.1233 & 0.4483\\ 0.3105 & 0.2989 & -0.4532 & 0.3090 & -0.3967 & 0.3090\end{bmatrix}$
				50		0.2251	$\begin{bmatrix}0.4622 & 0.4569 & -0.7458 & 0.4633 & 0.1682 & 0.4633\\ 0.3800 & 0.3741 & -0.1894 & 0.3814 & -0.3066 & 0.3814\end{bmatrix}$
				100		0.2251	$\begin{bmatrix}0.4755 & 0.4671 & -0.7537 & 0.4764 & 0.2081 & 0.4764\\ 0.3353 & 0.3332 & -0.2701 & 0.3378 & -0.3983 & 0.3378\end{bmatrix}$
				200		0.2251	$\begin{bmatrix}0.5005 & 0.4884 & -0.7722 & 0.5011 & 0.2832 & 0.5011\\ 0.2856 & 0.2856 & -0.4027 & 0.2883 & -0.4555 & 0.2883\end{bmatrix}$
3	100	0.215	5	0	0.225	0.2251	$\begin{bmatrix}0.4221 & 0.4385 & -0.8052 & 0.4255 & 0.0736 & 0.4255\\ 0.2444 & 0.2404 & -0.5265 & 0.2443 & -0.5731 & 0.2443\end{bmatrix}$
				50		0.2251	$\begin{bmatrix}0.4383 & 0.4475 & -0.8110 & 0.4418 & 0.1233 & 0.4418\\ 0.3460 & 0.3380 & -0.2890 & 0.3475 & -0.3334 & 0.3475\end{bmatrix}$
				100		0.2251	$\begin{bmatrix}0.4502 & 0.4548 & -0.8163 & 0.4534 & 0.1589 & 0.4534\\ 0.3206 & 0.3173 & -0.3288 & 0.3241 & -0.3864 & 0.3241\end{bmatrix}$
				200		0.2251	$\begin{bmatrix}0.4696 & 0.4690 & -0.8280 & 0.4721 & 0.2160 & 0.4721\\ 0.2726 & 0.2722 & -0.4403 & 0.2761 & -0.4626 & 0.2761\end{bmatrix}$
3	200	0.215	5	0	0.225	0.2251	$\begin{bmatrix}0.3977 & 0.4281 & -0.8147 & 0.4057 & 0.0051 & 0.4057\\ 0.2625 & 0.2621 & -0.4512 & 0.2639 & -0.6473 & 0.2639\end{bmatrix}$
				50		0.2251	$\begin{bmatrix}0.3995 & 0.4300 & -0.8172 & 0.4104 & 0.0144 & 0.4104\\ 0.2882 & 0.2805 & -0.4031 & 0.2903 & -0.4424 & 0.2903\end{bmatrix}$
				100		0.2251	$\begin{bmatrix}0.4177 & 0.4415 & -0.8276 & 0.4282 & 0.0727 & 0.4282\\ 0.2732 & 0.2699 & -0.4254 & 0.2783 & -0.4719 & 0.2783\end{bmatrix}$
				200		0.2251	$\begin{bmatrix}0.4398 & 0.4534 & -0.8366 & 0.4485 & 0.1387 & 0.4485\\ 0.2316 & 0.2314 & -0.5255 & 0.2356 & -0.5378 & 0.2356\end{bmatrix}$

3) Signals with Noise

This subsection presents the detection of secondary faults under noisy conditions. The faults occur in feeders 1 and 2. The Gaussian white noise (10-70 dB) is added to the simulation signal. The results in Table III show that the proposed method detects secondary faults correctly subjected to different noise conditions, and hence exhibits good anti-noise performance.

4) Secondary Fault Time with Error

The time at which the secondary fault occurs is detected using the WSE. The result shows that the detected time deviated from the actual fault time. As shown in Table I, when the secondary fault occurs at 0.223 s, the time detected by the WSE is 0.2238 s. The error is due to the length of the moving window used for the detection. We have tested the effect of the secondary fault-time error on the proposed feeder identification method. As shown in Table IV, if a second-

ary fault is detected before the actual fault time, the results of the feeder identification process are not affected by the time error. In reality, after being divided, the second fault stage includes the information of the secondary fault under that condition.

TABLE III
DETECTION RESULTS OF SECONDARY FAULTS WITH NOISE

Parameters	Noise (dB)	***PP***
$F_1=1$, $R_1=50\ \Omega$, $T_1=0.215$ s; $F_2=2$, $R_2=50\ \Omega$, $T_2=0.225$ s	No	$\begin{bmatrix}-0.9575 & 0.5336 & 0.5835 & 0.5815 & 0.5839 & 0.5815\\ -0.4206 & -0.2550 & 0.3335 & 0.3385 & 0.3400 & 0.3385\end{bmatrix}$
	70	$\begin{bmatrix}-0.9575 & 0.5336 & 0.5835 & 0.5815 & 0.5839 & 0.5815\\ -0.4205 & -0.2549 & 0.3335 & 0.3385 & 0.3401 & 0.3385\end{bmatrix}$
	60	$\begin{bmatrix}-0.9575 & 0.5336 & 0.5835 & 0.5815 & 0.5839 & 0.5816\\ -0.4209 & -0.2550 & 0.3336 & 0.3386 & 0.3399 & 0.3382\end{bmatrix}$
	50	$\begin{bmatrix}0.9573 & 0.5336 & 0.5835 & 0.5818 & 0.5839 & 0.5816\\ -0.4203 & -0.2546 & 0.3331 & 0.3384 & 0.3405 & 0.3392\end{bmatrix}$
	40	$\begin{bmatrix}-0.9574 & 0.5335 & 0.5835 & 0.5814 & 0.5840 & 0.5817\\ -0.4200 & -0.2550 & 0.3331 & 0.3375 & 0.3413 & 0.3386\end{bmatrix}$
	30	$\begin{bmatrix}-0.9583 & 0.5347 & 0.5839 & 0.5813 & 0.5832 & 0.5806\\ -0.4173 & -0.2609 & 0.3303 & 0.3407 & 0.3368 & 0.3343\end{bmatrix}$
	20	$\begin{bmatrix}-0.9540 & 0.5297 & 0.5798 & 0.5776 & 0.5816 & 0.5741\\ -0.4118 & -0.2364 & 0.3471 & 0.3391 & 0.3030 & 0.3289\end{bmatrix}$
	10	$\begin{bmatrix}-0.9043 & 0.4793 & 0.5185 & 0.5268 & 0.5116 & 0.5059\\ -0.4410 & -0.2766 & 0.2578 & 0.2928 & 0.3037 & 0.2711\end{bmatrix}$

However, if the time at which the secondary fault is detected lags behind the actual fault time, the error may affect the accuracy of identification of the secondary fault feeder. As shown in Table IV, when the fault resistance is 0 Ω, all cases in which the detected fault time lags behind the actual fault time result in a correct identification of the fault feeders. When the fault resistance is 100 Ω and the time at which the secondary fault is detected lags by 2% or 3%, the secondary fault feeder could not be identified. In fact, the transient of the secondary fault is attenuated substantially in the data window at the second fault stage because of the error in the time at which the secondary fault is detected, so that the information associated with the fault transient is insufficient for identifying the secondary fault feeder. This issue is particularly significant for conditions involving high fault resistance values. Since the fault transient is weak, the possibility of misidentifying the feeder fault is increased.

V. CONCLUSION

A fault feeder identification method that considers secondary earth faults in a non-effectively grounded system is proposed herein. The proposed method can be categorized into two processes: fault time detection of secondary earth faults using WSE, and fault feeder identification using a time-frequency similarity matrix. A simulation model with six feeders of a resonant grounded system in PSCAD/EMTDC is used to test the proposed method. The simulation results indicate that the proposed method can overcome the effects of differences in the initial phase angle and fault resistance. Moreover, the method demonstrates excellent anti-noise ability.

TABLE IV
DETECTION RESULTS OF SECONDARY FAULT TIME WITH ERROR

Parameters	Time error (%)	T (s)	***PP***
$F_1=6$, $R_1=0\ \Omega$, $T_1=0.215$ s; $F_2=1$, $R_2=0\ \Omega$, $T_2=0.242$ s	0.0	0.2420	$\begin{bmatrix}0.4428 & 0.5217 & 0.5416 & 0.5414 & 0.5410 & -0.9172\\ -0.7839 & 0.6370 & 0.6367 & 0.6370 & 0.6372 & 0.5574\end{bmatrix}$
	−0.5	0.2408	$\begin{bmatrix}0.4428 & 0.5217 & 0.5416 & 0.5414 & 0.5410 & -0.9172\\ -0.8612 & 0.6205 & 0.6203 & 0.6205 & 0.6206 & 0.5534\end{bmatrix}$
	−1.0	0.2396	$\begin{bmatrix}0.4428 & 0.5217 & 0.5416 & 0.5414 & 0.5410 & -0.9172\\ -0.8277 & 0.6204 & 0.6202 & 0.6204 & 0.6205 & 0.5168\end{bmatrix}$
	−2.0	0.2372	$\begin{bmatrix}0.4428 & 0.5217 & 0.5416 & 0.5414 & 0.5410 & -0.9172\\ -0.4104 & 0.6787 & 0.6785 & 0.6788 & 0.6786 & 0.3681\end{bmatrix}$
	−3.0	0.2347	$\begin{bmatrix}0.4428 & 0.5217 & 0.5416 & 0.5414 & 0.5410 & -0.9172\\ -0.7957 & 0.6245 & 0.6244 & 0.6246 & 0.6246 & 0.5033\end{bmatrix}$
	0.5	0.2432	$\begin{bmatrix}0.4428 & 0.5217 & 0.5416 & 0.5414 & 0.5410 & -0.9172\\ -0.5803 & 0.6769 & 0.6766 & 0.6769 & 0.6773 & 0.5545\end{bmatrix}$
	1.0	0.2444	$\begin{bmatrix}0.4428 & 0.5217 & 0.5416 & 0.5414 & 0.5410 & -0.9172\\ -0.1284 & 0.7493 & 0.7489 & 0.7493 & 0.7497 & 0.4601\end{bmatrix}$
	2.0	0.2468	$\begin{bmatrix}0.4428 & 0.5217 & 0.5416 & 0.5414 & 0.5410 & -0.9172\\ -0.2254 & 0.6785 & 0.6782 & 0.6786 & 0.6788 & 0.1739\end{bmatrix}$
	3.0	0.2493	$\begin{bmatrix}0.4428 & 0.5217 & 0.5416 & 0.5414 & 0.5410 & -0.9172\\ -0.7901 & 0.6274 & 0.6271 & 0.6274 & 0.6277 & 0.5118\end{bmatrix}$
$F_1=6$, $R_1=100\ \Omega$, $T_1=0.215$ s; $F_2=1$, $R_2=100\ \Omega$, $T_2=0.223$ s	0.0	0.2230	$\begin{bmatrix}0.3868 & 0.4571 & 0.4970 & 0.5133 & 0.4968 & -0.8132\\ -0.5905 & 0.6501 & 0.6528 & 0.6539 & 0.6532 & 0.6470\end{bmatrix}$
	−0.5	0.2219	$\begin{bmatrix}0.5142 & 0.4248 & 0.5417 & 0.5473 & 0.5400 & -0.8553\\ -0.7756 & 0.6347 & 0.6376 & 0.6375 & 0.6373 & 0.5845\end{bmatrix}$
	−1.0	0.2208	$\begin{bmatrix}0.4821 & 0.4103 & 0.5246 & 0.5349 & 0.5239 & -0.8346\\ -0.4339 & 0.6579 & 0.6603 & 0.6601 & 0.6600 & 0.3234\end{bmatrix}$
	−2.0	0.2185	$\begin{bmatrix}0.4205 & 0.2023 & 0.4436 & 0.4733 & 0.4451 & -0.7999\\ -0.3170 & 0.5457 & 0.5613 & 0.5635 & 0.5597 & -0.1461\end{bmatrix}$
	−3.0	0.2163	$\begin{bmatrix}0.2934 & 0.0090 & 0.3561 & 0.3757 & 0.3583 & -0.6837\\ -0.4955 & 0.4754 & 0.4707 & 0.4717 & 0.4727 & -0.2391\end{bmatrix}$
	0.5	0.2241	$\begin{bmatrix}0.2923 & 0.4777 & 0.4984 & 0.4956 & 0.4981 & -0.8449\\ -0.4334 & 0.6917 & 0.7005 & 0.6997 & 0.7012 & 0.7256\end{bmatrix}$
	1.0	0.2252	$\begin{bmatrix}0.2674 & 0.4925 & 0.5116 & 0.5087 & 0.5117 & -0.7843\\ -0.4905 & 0.6975 & 0.6956 & 0.6947 & 0.6961 & 0.7122\end{bmatrix}$
	2.0	0.2275	$\begin{bmatrix}0.2050 & 0.5140 & 0.5301 & 0.5264 & 0.5303 & -0.7040\\ 0.4084 & 0.8648 & 0.8657 & 0.8634 & 0.8534 & 0.8839\end{bmatrix}$
	3.0	0.2297	$\begin{bmatrix}0.1501 & 0.5053 & 0.5218 & 0.5180 & 0.5214 & -0.6806\\ 0.9811 & 0.9959 & 0.9959 & 0.9959 & 0.9957 & 0.9967\end{bmatrix}$

However, if the time at which the secondary fault is detected lags behind the actual fault time by 2% or more, the accuracy of secondary fault feeder identification may be affected. Therefore, by reducing the time window length to improve the detection accuracy of the secondary fault time, the misidentification of a fault feeder with a secondary fault can be reduced.

REFERENCES

[1] J. Chen, E. Chu, Y. Li *et al.*, "Faulty feeder identification and fault area localization in resonant grounding system based on wavelet packet and bayesian classifier," *Journal of Modern Power Systems and Clean Energy*, vol. 8, no. 4, pp. 760-767, Jul. 2020.

[2] T. Zhang, C. Wang, F. Luo *et al.*, "Analytical calculation method of reliabilty sensitivity indexes for distribution systems based on fault incidence matrix," *Journal of Modern Power Systems and Clean Energy*, vol. 8, no. 2, pp. 325-333, Mar. 2020.

[3] Y. Wang, X. Yin, W. Xu *et al.*, "Fault line selection in cooperation with multi-mode grounding control for the floating nuclear power

plant grid," *Protection and Control of Modern Power Systems*, vol. 5, no. 16, pp. 1-10, Jul. 2020.
[4] S. Zhang, Z. He, and R. Mai, "Single-phase-to-ground fault feeder identification based on the feature between voltage and integration of current," *IEEJ Transactions on Electrical and Electronic Engineering*, vol. 12, pp. 683-691, May 2017.
[5] X. Lin, J. Sun, I. Kursan *et al*., "Zero-sequence compensated admittance based faulty feeder selection algorithm used for distribution network with neutral grounding through Peterson-coil," *Electrical Power and Energy Systems*, vol. 63, pp.747-752, Jun. 2014.
[6] Y. Du, Y. Liu, Q. Shao *et al*., "Single line-to-ground faulted line detection of distribution systems with resonant grounding based on feature fusion framework," *IEEE Transactions on Power Delivery*, vol. 34, no. 4, pp. 1766-1775, Aug. 2019.
[7] P. Liu and C. Huang, "Detecting single-phase-to-ground fault event and identifying faulty feeder in neutral ineffectively grounded distribution system," *IEEE Transactions on Power Delivery*, vol. 33, no.5, pp. 2265-2272, Oct. 2018.
[8] X. Dong and S. Shi, "Identifying single-phase-to-ground fault feeder in neutral non-effectively grounded distribution system using wavelet transform," *IEEE Transactions on Power Delivery*, vol. 23, no.4, pp. 1829-1837, Oct. 2008.
[9] H. Hasanvand and A. Parastar, "A comparison between S-transform and CWT for fault location in combined overhead line and cable distribution networks," in *Proceedings of 21st Electrical Power Distribution Networks Conference*, Karaj-Alborz, Iran, May 2016, pp. 70-74.
[10] X. Han, Q. Wu, M. Li *et al*., "Mathematical morphology-based single phase-to-ground fault feeder selector for a resonant grounded distribution system," *IEEJ Transactions on Electrical and Electronic Engineering*, vol. 13, pp. 517-518. May 2018.
[11] Z. Guo, J. Yao, and Z. Tan, "Hilbert-Huang transform-based transient busbar protection algorithm," *IET Generation, Transmission & Distribution*, vol. 9, no. 4, pp. 2032-2039, Oct. 2015.
[12] Y. Xue, X. Chen, H. Song *et al*., "Resonance analysis and faulty feeder identification of high-impedance faults in resonant grounding system," *IEEE Transactions on Power Delivery*, vol. 32, no. 3, pp. 1545-1555, Jan, 2017.
[13] M. Guo, S. Liu, and G. Yang, "A novel approach to detect fault lines in distribution network using similarity recognition based on time-frequency spectrum," *Proceeding of the CSEE*, vol. 33, no. 19, pp. 183-190, Oct. 2013.
[14] I. Kiaei and S. Lotfifard, "Fault section identification in smart distribution systems using multi-source data based on fuzzy Petri nets," *IEEE Transactions on Smart Grid*, vol. 11, no. 1, pp. 74-83, Jan. 2020.
[15] X. Wang, J. Gao, M. Chen *et al*., "Faulty line detection method based on optimized bistable system for distribution network," *IEEE Transactions on Industrial Informatics*, vol. 14, no. 4, pp. 1370-1380, Apr. 2018.
[16] W. Zhang, G. Song, M. Wu *et al*., "Application of parameter identification in secondary single-phase grounding fault detection of 10 kV small current grounding system," *Distribution & Utilization*, vol. 4, pp. 72-78, Jun. 2017.
[17] B. Jiang, X. Dong, and S. Shi, "Application of approximate entropy to cross-country fault detection in distribution network," *Power System Protection and Control*, vol. 43, no. 17, pp. 15-21, Sept. 2015.
[18] A. Codino, F. M. Gatta, and R. Calone, "Detection of cross-country faults in medium voltage distribution ring lines," in *Proceedings of 2017 AEIT International Annual Conference*, Cagliari, Italy, Sept. 2017, pp. 1-6.
[19] R. Burgess and A. Ahfock, "Minimizing the risk of cross-country faults in systems using arc suppression coils," *IET Generation, Transmission & Distribution*, vol. 5, no.7, pp. 703-711, Jul. 2011.
[20] J. Wang, "The fault detection of the simultaneous SLG in two distribution feeders," *Heilongjiang Power Technology*, vol. 13, no. 5, pp. 281-282, May 1999.
[21] X. Dong, B Su, and S. Shi, "Cross-country disturbance information and its application in relay protection," *Automation of Electric Power Systems*, vol. 28, no. 2, pp. 21-25, Jan. 2004.
[22] Y. Xue, Y. Xie, and F. Wen, "A review on cascading failures in power systems," *Automation of Electric Power Systems*, vol. 37, no. 19, pp. 1-9, Oct. 2013.
[23] Z. He, X. Chen, and G. Luo, "Wavelet entropy measure definition and its application for transmission line fault detection and identification (part i: definition and methodology)," in *Proceedings of 2006 International Conference on Power System Technology*, Chongqing, China, Oct. 2006, pp. 22-26.
[24] N. Peng, K. Ye, R. Liang *et al*., "Single-phase-to-earth fault feeder detection in power distribution network based on amplitude ratio of zero-mode transients," *IEEE Access*, vol. 7, pp. 117678-117691, Aug. 2019.
[25] R. Liang, N. Peng, Z. Yang *et al*., "A novel single-phase-to-earth fault location method for distribution network based on zero-sequence components distribution characteristics," *International Journal of Electrical Power and Energy Systems*, vol. 102, pp. 11-22, Nov. 2018.
[26] M. G, S. Liu, and G. Yang, "A new approach to detect fault lines in distribution network using similarity recognition based on time-frequency spectrum," *Proceeding of the CSEE*, vol. 33, no. 19, pp. 183-190, Oct. 2013.

Shu Zhang received the B.S., M.S., and Ph.D. degrees in electrical engineering from Southwest Jiaotong University, Chengdu, China, in 2010, 2013, and 2018, respectively. Currently, she is a Research Assistant in the College of Electrical Engineering, Sichuan University, Chengdu, China. Her research interests include fault diagnosis and automation of distribution network, load analysis, and modelling by power disturbance data.

Tianlei Zang received the Ph.D. degree from Southwest Jiaotong University, Chengdu, China, in 2017. From 2017 to 2020, he was a Postdoctoral Researcher with Tsinghua University, Beijing, China. Currently, he is an Associate Research Fellow with the College of Electrical Engineering, Sichuan University, Chengdu, China. His research interests include energy internet, fault analysis, and safety assessment of energy electrical systems.

Wenhai Zhang received the B.S. and Ph.D. degrees in electrical engineering from Sichuan University, Chengdu, China, in 2010 and 2016, respectively. Since 2018, he has been a Research Assistant with the College of Electrical Engineering, Sichuan University, Chengdu, China. From September 2014 to September 2015, he was a visiting Ph.D. student with the University of Alberta, Edmonton, Canada. From 2016 to 2018, he was a Senior Engineer with the State Grid Sichuan Maintenance Company, Chengdu, China. His current research interests include condition monitoring, fault diagnosis, incipient fault detection and location, and power disturbance analytics.

Xianyong Xiao received the B.S., M.S., and Ph.D. degrees in electrical engineering from Sichuan University, Chengdu, China, in 1990, 1998, and 2010, respectively. Currently, he is a Professor in the College of Electrical Engineering at Sichuan University. His research interests include power quality, smart distribution systems, power system catastrophic events, uncertainty theory, and uncertainty measures applied to power systems.